

Modeling and Implementation of Space Vector PWM Driver of 3-Phase Induction Motor

Dr. Majid K. Al-Khatat* & Fadhil Abbas Hassan* 

Received on: 27/7/2008

Accepted on: 5/3/2009

Abstract

This research proposes the design, simulation, and implementation of a three-phase induction motor driver, using voltage-fed Space Vector Pulse Width Modulation technique (SVPWM), which is an advance and modern technique. The SVPWM provides maximum usage of the DC link. A MATLAB/SIMULINK program is prepared for simulating the overall drive system which include; voltage-fed space vector PWM inverter model and three-phase induction motor model. A practical model is designed by imitate the conceptions of TMS320 (DSP) microcontroller. This practical model is completely implemented and exact results are obtained. The worst state of the harmonics content of the voltage and current (no-load condition) are analyzed. This analysis shows high reduction in the dominant harmonics and very low total harmonic distortion (THD) when SVPWM is used (less than 5%), compared to (more than 20%) in square wave. Experimental and simulation results have verified the superior performance and the effectiveness in reduction the harmonic losses and switching losses.

Keywords: SVPWM, Harmonics Analysis, Dynamic Model of Induction Motor, DSP, Design and Implementation, THD.

نموذج وتنفيذ لسوافة مضمن عرض النبضة للمتجه الفضائي لمحرك حثي ثلاثي الطور

الخلاصة

يقدم هذا البحث التصميم و التمثيل و التطبيق لسوافة محرك حثي ثلاثي الطور بأستخدام مغذي جهد بتقنية تضمين عرض النبضة للمتجه الفضائي. تعتبر هذه التقنيه من اكثر الطرق المتقدمه والحديثه. أن مضمن المتجه الفضائي يوفر أقصى أستفادة من الجهد المستمر. لغرض محاكاة النموذج الرياضي لكامل المنظومة تم أستخدام برنامج MATLAB/SIMULINK والذي يتألف (النموذج) من: النموذج التمثيلي لمغذي الجهد ذو تقنية تضمين عرض النبضة للمتجه الفضائي والنموذج التمثيلي للمحرك الحثي ثلاثي الطور. تم تصميم نموذج عملي لمنظومة التضمين للمتجه الفضائي عن طريق محاكاة طريقة عمل المعالج الدقيق TMS320. وقد أظهر التصميم الكامل للمنظومة أداءً مثالياً. وبتحليل التوافقيات المتضمنة في إشارة التيار والجهد لعدة سرع وفي أسوء الظروف (التشغيل في

* Electrical and Electronic Engineering Department, University of Technology / Baghdad

اللاحمل) ، أظهر مضمن المتجه الفضائي أداءً ممتازاً في تخفيض قيم التوافقيات الرئيسية وقيم قليلة جداً لمعامل التشويه التوافقي حيث يكون أقل من (5%) مقارنة بأعلى من (20%) في الموجه المربعة. أن نتائج الأختبار العملي والتمثيل الرياضي أثبتت وبشكل واضح الأداء الفائق والفاعلية الكبيرة في تخفيض خسائر التحويل وخسائر التوافقيات.

1. Introduction

Variable-voltage variable-frequency inverter drives are the most important method used as speed control of induction motors. For long time a square wave inverter used as speed control of low- and medium-power induction motor [1,2], which consist of variable AC to DC converter produces controllable DC voltage which is used to generate single, two or three phase output square wave at variable frequency, using semiconductor devices like transistors or thyristors. The main disadvantage of this method is the high number of harmonics, which causes many operation problems.

After the developments in power electronic technology, the pulse width modulation technique appears which minimized harmonic effects. In PWM inverter the DC link kept constant by a front end diodes bridge and the fundamental output frequency can be controlled within the inverter using PWM technique, the inverter power bridge devices switched "on" and "off" many times within half-cycle in order to generate variable output voltage which has low harmonics content used as speed control of a few hundreds of Kw induction motors [3].

At present time, fully digital AC drives becoming an industrial standard and high performance drives represents by space vector pulse width modulation (SVPWM), which become a good solution for many modulation problems presented in traditional PWM. This method based on fully digital signal processing which produces high performance

output voltage with low harmonics to fundamental ratio.

2. Voltage source inverter

A voltage source inverter (VSI) should have a stiff voltage source at the input, that is, its Thevenin impedance should ideally be zero. Thus, a large capacitor can be connected to the input if the voltage source is not stiff. Figure (1) shows a practical (VSI) consist of power bridge devices with three output legs, each consisting of two power switches and two freewheeling diodes, the inverter is supplied from DC voltage source (either battery or diode-based bridge rectifier) via LC or C filter.

In (VSI) the power semiconductor devices always remain forward biased due to the DC supply voltage, therefore, self-controlled forward or asymmetric blocking devices, such as GTOs, BJTs, IGBTs and power MOSFETs are suitable. One important characteristic of the (VSI) is that the AC fabricated voltage wave is not affected by the load parameters [1,5].

3. SVPWM technique

Since digital AC drives are becoming popular in industry, the traditional triangular carrier method has been overcome by the SVPWM. Because of its superior performance characteristics, it has been finding widespread applications in recent years. With PWM, the inverter can thought as three separate push-pull drive stages, which create each phase

waveform independently. However, SVPWM treats the inverter as single unit [1,2,3].

With a machine load, the load neutral is normally isolated, which causes interaction among the phases. This interaction was not considered before in PWM. The SVPWM method considers this interaction of the phases and optimizes the harmonics of three-phase isolated neutral load [1].

3.1 Switching states vector:

A three-phase bridge inverter, as shown in figure (1), with three output legs, has (2³ = 8) permissible switching states. If leg(a) which connected between (Q₁,Q₄) is represented by an indicator “S_a”, also leg(b) by an indicator “S_b” and leg(c) by “S_c”, since the upper switching devices and the lower switching devices are complementary (i.e. Q₄ = 1 - Q₁), then, the switching states can be represented by binary values (0,1). When, S_a= 0 that equal to Q₁= off and Q₄= on, when S_a= 1 that equal to Q₁=on and Q₄= off, and that is true for S_b and S_c . The eight switching states of the three-phase inverter can be shown in figure (2) [1,2,3,6].

The relationship between the switching variable vector [S_a , S_b , S_c]^T and the line-to-line output voltage vector [V_{ab}, V_{bc}, V_{ca}]^T and the phase voltage vector [V_{an}, V_{bn} , V_{cn}]^T are given by the following equations [1,2]:

$$\begin{bmatrix} V_{ab} \\ V_{bc} \\ V_{ca} \end{bmatrix} = V_d \begin{bmatrix} 1 & -1 & 0 \\ 0 & 1 & -1 \\ -1 & 0 & 1 \end{bmatrix} \begin{bmatrix} S_a \\ S_b \\ S_c \end{bmatrix} \dots(1)$$

$$\begin{bmatrix} V_{an} \\ V_{bn} \\ V_{cn} \end{bmatrix} = \frac{1}{3} V_d \begin{bmatrix} 2 & -1 & -1 \\ -1 & 2 & -1 \\ -1 & -1 & 2 \end{bmatrix} \begin{bmatrix} S_a \\ S_b \\ S_c \end{bmatrix} \dots(2)$$

Where, V_d is the DC supply of the inverter bridge.

By applying the eight states of [S_a , S_b , S_c]^T in equations (2) gives the line-to-neutral voltages space vectors shown in table (1).

3.2 Space vector representation

To understand the SVPWM theory, the concept of a rotating space vector and axis transformation is very important [1,2,3]. Any three-phase quantities can be represented by two axis frames, like (qd) axes which are a complex axis frame, q-axis represents quadrature real axis and d-axis represents direct imaginary axis. The transformation procedure can easily be done by the following formula [1,2,3,6]:

$$\begin{bmatrix} V_q \\ V_d \end{bmatrix} = \frac{2}{3} \begin{bmatrix} \cos 0 & \cos 120^\circ & \cos -120^\circ \\ \sin 0 & \sin 120^\circ & \sin -120^\circ \end{bmatrix} \begin{bmatrix} V_a \\ V_b \\ V_c \end{bmatrix}$$

Or,

$$\begin{bmatrix} V_q \\ V_d \end{bmatrix} = \frac{2}{3} \begin{bmatrix} 1 & -1/2 & -1/2 \\ 0 & \sqrt{3}/2 & -\sqrt{3}/2 \end{bmatrix} \begin{bmatrix} V_a \\ V_b \\ V_c \end{bmatrix}$$

The resultant voltage space vector is given by:

$$\begin{aligned} V_{qd} &= V_q + jV_d \\ &= \frac{2}{3} [(V_a - \frac{1}{2}V_b - \frac{1}{2}V_c) + j(\frac{\sqrt{3}}{2}V_b + \frac{-\sqrt{3}}{2}V_c)] \\ &= \frac{2}{3} [V_a + (-\frac{1}{2} + j\frac{\sqrt{3}}{2})V_b + (-\frac{1}{2} - j\frac{\sqrt{3}}{2})V_c] \\ V_{qd} &= \frac{2}{3} [V_a + aV_b + a^2V_c] \dots(3) \end{aligned}$$

Where, a = e^{j120°} and a²= e^{-j120°}.

By applying the phase and line voltages of different states in equation (3) phase and magnitude of the eight

switching space vector voltage can be gotten as shown in table (2).

Table (2) shows that there are six non-zero space vectors and two zero space vectors. The active vectors are 60° angle apart and describe a hexagon boundary with six sectors as shown in figure (3).

The two zero vectors $V_0(000)$ & $V_7(111)$ are represented as two dots at the origin. The desired three-phase voltage called reference voltage “ V_{ref} ” as shown in figure (3), the magnitude and rotational speed of “ V_{ref} ” is the same as the fundamental magnitude and frequency. If the output space vector “ V_{ref} ” moves through the six states $V_1 \rightarrow V_6$ the output voltage will have square waveform [1].

In SVPWM the space reference voltage moves from state-1 to state-2 by time sharing PWM between V_1 and V_2 . For example if the vector “ V_{ref} ” lies in sector-1, the PWM adjusted between $V_1(100)$ and $V_2(110)$ by duty cycle of each being T_a and T_b respectively, and the zero vectors $V_0(000)$ and $V_7(111)$ of duty cycle T_o [1,2]:

$$\int_0^{T_s} V_{ref} dt = \int_0^{T_a} V_1 dt + \int_{T_a}^{T_a+T_b} V_2 dt + \int_{T_a+T_b}^{T_s} V_o \text{ or } (V_7) dt$$

$$T_s V_{ref} = T_a V_1 + T_b V_2 + T_o V_o \dots\dots(4)$$

$$T_s = T_a + T_b + T_o \dots\dots(5)$$

Where, T_s is the sampling time period of the switching frequency.

Usually, each sector of the hexagon is divided into sub-sectors in which the reference voltage “ V_{ref} ” will moves in angular steps, the width

of steps (sub-sector angle) depends on the maximum permissible switching rate of the power switching devices. whenever step width is small and switching rate is high the shape of the output fundamental voltage will be close to sine wave but with increase in the switching losses [6,7].

3.3 Modulation regions

3.3.1 Linear or undermodulation region:

In this region the inverter transfer characteristics are naturally linear and the reference space voltage has continues rotation [1,8]. Figure (4) shows phase (a) component of the reference voltage in six sectors. As an example, a convenient way to generate the PWM output is to use the space vectors V_1 and V_2 of sector-1 on apart-time basis to satisfy the average output demand as shown in figure (4):

$$V_{ref} \sin (60^\circ - \theta) = V_a \sin(60^\circ)$$

$$V_{ref} \sin (\theta) = V_b \sin (60^\circ)$$

- $V_a = \frac{2}{\sqrt{3}} V_{ref} \sin (60^\circ - \theta)$

$$V_b = \frac{2}{\sqrt{3}} V_{ref} \sin (\theta)$$

$$V_{ref} = V_a + V_b = V_1 \frac{T_a}{T_s} + V_2 \frac{T_b}{T_s} + V_o \frac{T_o}{T_s}$$

- $T_a = \frac{V_a}{V_1} T_s \quad ; \quad V_1 = \frac{2V_d}{3}$

$$T_b = \frac{V_b}{V_2} T_s \quad ; \quad V_2 = \frac{2V_d}{3}$$

$$T_o = T_s - T_a - T_b$$

That led to:

$$T_a = \sqrt{3} T_s \frac{V_{ref}}{V_d} \sin (60^\circ - \theta) \dots\dots(6)$$

$$T_b = \sqrt{3} T_s \frac{V_{ref}}{V_d} \sin(\theta) \dots(7)$$

$$T_o = T_s - (T_a + T_b) \dots(8)$$

The time interval T_a and T_b satisfy the reference voltage, but T_o fills up the remaining gap in T_s [1].

In the linear region the vector V_{ref} always remains within the hexagon. The region ends when V_{ref} equal to the radius of biggest circle can be drawn within the hexagon as shown in figure (4). The ratio between the reference vector V_{ref} and the fundamental peak value of the square-phase voltage wave ($\frac{2V_d}{\pi}$) called the modulation index (m):

$$m = \frac{V_{ref}}{V_{1sw}} \dots(9)$$

The maximum modulation index can be obtained when V_{ref} equal to the radius of the inscribed circle:

$$(V_{ref})_{max} = \frac{2}{3} V_d \cos(30^\circ) = 0.577 V_d$$

Therefore,

$$m_{max} = \frac{0.577 V_d}{2V_d/\pi} = 0.907$$

It means that 90.7 percent of the square wave fundamental voltage is available in the linear region of SVPWM.

3.3.2 Overmodulation region mode-1:

In overmodulation region mode-1, shown in figure (5) the reference voltage V_{ref} crosses the hexagon

boundary at two points in each sector. There will be loss of fundamental voltage in the part where the reference vector exceeds the hexagon boundary. In the circular part of the trajectory T_a , T_b & T_o can be calculated using equations (6) (7) (8). But, when V_{ref} exceeds the hexagon trajectory, the zero time T_o vanishes, giving only T_a , T_b time intervals and they can be calculated by [1,2]:

$$T_a = T_s \left[\frac{\sqrt{3} \cos(\theta) - \sin(\theta)}{\sqrt{3} \cos(\theta) + \sin(\theta)} \right] \dots(10)$$

$$T_b = T_s - T_a \dots(11)$$

The angle of the circular part of trajectory called the crossover angle " α_c " as shown in figure (5).

The crossover angle (α_c) has standard values depend on the value of the modulation index " m ", it's vary between 30° at the beginning of mode-1 when " $m = 0.907$ ", and 0° at the end of mode-1 when " $m = 0.952$ ".

3.3.3 Overmodulation region mode-2:

When the modulation index increases further up to 0.952, overmodulation mode-2 will be reached, tending toward square-wave mode operation as shown in figure (6). this mode characterized by partly holding the modified vector at the hexagon corners for holding angle " α_h " and partly by tracking the hexagon sides in every sector [1,2]. During the holding angle, the magnitude of V_{an} remains constant, whereas during hexagon tracking, the voltage changes approximately in linear manner, as shown in figure (6). Mode-2 ends when $\alpha_h = 30^\circ$, the linear segments vanish, giving

square-wave output voltage at modulation index $m = 1$.

4. System simulation:

4.1 SVPWM program:

In order to calculate the time periods T_a, T_b, T_o and generate the corresponding states vector $[S_a, S_b, S_c]^T$, a MATLAB program was written, the main features of this program are:

a . Receives the input data (V_{com}, f_e and θ_e) then, calculate T_{period} & T_s :

$$T_{period} = \frac{T_{rated}}{m} = \frac{1/50}{m} = \frac{0.02}{m}$$

(sec.)

$$T_s = \frac{T_{sector}}{\text{no. of sub-sectors}}$$

$$= \frac{T_{period} / 6}{6} = \frac{0.02}{36 * m}$$

(sec.)

Where, m is the modulation index.

b . Limits the value of θ_e between 0° to 60° in each sector, and indicate sector number.

c . Checks the value of the modulation index.

■ If $m \leq 0.907$ calculates T_a, T_b, T_o using equations (6), (7), (8).

■ If $0.907 < m \leq 0.952$, estimates the value of crossover angle from the standard table, then calculates T_a, T_b, T_o according to the rules of overmodulation mode-1 and equations (10), (11).

■ If $m > 0.952$, estimates the value holding angle, then calculates T_a, T_b, T_o according to the rules of overmodulation mode-2.

d . Generates the state vector $[S_a, S_b, S_c]^T$ according to the time intervals of each sector by using internal timer. Figure (7) shows the flow chart of the program.

Simply, after generating the state vector $[S_a, S_b, S_c]^T$, the output three-phase voltage can be obtained by using equation (2). The final SVPWM sub-system simulation can be shown in figures (8).

4.2 Induction motor model:

The steady state equivalent circuit of an induction motor is not suitable in our modeling, because it not deals with transient conditions in speed adjusting performance [1,7]. Thus, the dynamic model of the induction motor is used, it's look like as three-phase transformer with moving secondary coil at speed equal to the rotor speed, in which the coupling coefficients between the stator and the rotor changes continuously with the change of the rotor position " θ_r ". The machine model can be described by differential equations with time-varying mutual inductance. Such a model tends to be very complex [1,6], because of two problems:

- Complex differential equations.
- Time-varying parameters.

To solve these problems two procedures are essentially considered here. First, in order to simplify the model, the axis transformation method is used to transfer the three-phase stationary variables (a_s, b_s, c_s) to two phase stationary frame (d^s-q^s) as shown in figure (9).

The equation now is some what simple, but the problem of time-varying parameters still remains. The second procedure is called Park's transformation [1], by which the two-phase stationary variables (d^s-q^s) are transferred to synchronously rotating reference frame (d^e-q^e) fixed on the

rotor, which means the stator and rotor variables will rotate in the same speed and become constant to each other, the time-varying problem will vanished. The transformation procedure can be doing by the following equation [1]

$$\begin{bmatrix} V_q^e \\ V_d^e \end{bmatrix} = \begin{bmatrix} \cos \theta_e & -\sin \theta_e \\ \sin \theta_e & \cos \theta_e \end{bmatrix} \begin{bmatrix} V_q^s \\ V_d^s \end{bmatrix} \quad \dots(10)$$

Where, V_q^e & V_d^e are the synchronously rotating voltages. The simulation of the sub-system shown in figure (10).

4.2.1 Dynamic model of induction motor:

The machine dynamic model in state-space form is very important for transient analysis, especially for computer simulations studies. The electrical variables in the model can be chosen as flux, current, or mixture of both, the synchronously rotating frame state-space equations in (d^e-q^e) axis are [1]:

Stator q-axis current:

$$i_{qs}^e = \frac{F_{qs}}{x_s} - \frac{F_{qm}}{x_s} \quad \dots(11)$$

Rotor q-axis current:

$$i_{qr}^e = \frac{F_{qr}}{x_r} - \frac{F_{qm}}{x_r} \quad \dots(12)$$

Stator d-axis current:

$$i_{ds}^e = \frac{F_{ds}}{x_s} - \frac{F_{dm}}{x_s} \quad \dots(13)$$

Rotor d-axis current:

$$i_{dr}^e = \frac{F_{dr}}{x_r} - \frac{F_{dm}}{x_r} \quad \dots(14)$$

Stator q-axis induced EMF:

$$\frac{dF_{qs}}{dt} = \omega_b [v_{qs}^e - \frac{\omega_r}{\omega_b} F_{ds} - \frac{R_s}{x_s} (F_{qs} - F_{qm})] \quad \dots(15)$$

Stator d-axis induced EMF:

$$\frac{dF_{ds}}{dt} = \omega_b [v_{ds}^e + \frac{\omega_r}{\omega_b} F_{qs} - \frac{R_s}{x_s} (F_{ds} - F_{dm})] \quad \dots(16)$$

Rotor q-axis induced EMF:

$$\frac{dF_{qr}}{dt} = -\omega_b [(\frac{\omega_s}{\omega_b} - \frac{\omega_r}{\omega_b}) F_{dr} + \frac{R_r}{x_r} (F_{qr} - F_{qm})] \quad \dots(17)$$

Rotor d-axis induced EMF:

$$\frac{dF_{dr}}{dt} = -\omega_b [(\frac{\omega_s}{\omega_b} - \frac{\omega_r}{\omega_b}) F_{qr} + \frac{R_r}{x_r} (F_{dr} - F_{dm})] \quad \dots(18)$$

Where,

$$F_{qm} = \frac{x_{m1}}{x_s} F_{qs} + \frac{x_{m1}}{x_r} F_{qr} \quad \dots(19)$$

$$F_{dm} = \frac{x_{m1}}{x_s} F_{ds} + \frac{x_{m1}}{x_r} F_{dr} \quad \dots(20)$$

$$x_{m1} = 1 / (\frac{1}{x_s} + \frac{1}{x_r} + \frac{1}{x_m}) \quad \dots(21)$$

x_s : stator reactance, x_r : rotor reactance (referred to stator), R_s : stator resistance, R_r : rotor resistance (referred to stator), x_m : leakage reactance, ω_b : is electrical base speed (rated speed).

By simulate these equations the synchronous rotating frame dynamic model is gotten as shown in figure (11).

In order to calculate rotor speed and torque of the motor, the following equations are used [1]:

$$T_e = \frac{3}{2} (\frac{P}{2}) \frac{1}{\omega_b} (F_{ds} i_{qs}^e - F_{qs} i_{ds}^e) \quad \dots(22)$$

$$T_e = T_L + \frac{2}{P} J \frac{dw_r}{dt} \quad \dots(23)$$

$$\text{Or, } \frac{dw_r}{dt} = \frac{P}{2J} (T_e - T_L) \quad \dots(24)$$

Where, T_e is the electromagnetic torque, T_L is the load torque, J is the moment of inertia of the rotor and load, ω_r is the rotor electrical speed. By simulate these equations the rotor

parameters (T_e , ω_r) can be obtained as shown in figure (12).

4.2.2 3-phase stator current simulation:

In order to obtain the three-phase stator current, firstly it must transfer the 2-axis synchronously rotating current frame (i_{qd}^s) to 2-axis stationary current frame (i_{qd}^s) using inverse transformation equations [1]:

$$\begin{bmatrix} i_q^s \\ i_d^s \end{bmatrix} = \begin{bmatrix} \cos \theta_e & \sin \theta_e \\ -\sin \theta_e & \cos \theta_e \end{bmatrix} \begin{bmatrix} i_q^r \\ i_d^r \end{bmatrix} \dots\dots(25)$$

The simulation of this equation is shown in figure (13).

The second step is to transfer the 2-axis stationary current frame (i_{qd}^s) to

three-phase stationary current frame (i_{abc}), using inverse transformation equation [1,5]:

$$\begin{bmatrix} i_a \\ i_b \\ i_c \end{bmatrix} = \begin{bmatrix} 1 & 0 \\ -1/2 & \sqrt{3}/2 \\ -1/2 & -\sqrt{3}/2 \end{bmatrix} \begin{bmatrix} i_q^s \\ i_d^s \end{bmatrix} \dots\dots(26)$$

By simulate this equation the stator three-phase current are obtained as shown in figure (14).

Finally, by collection of all the previous sub-systems the overall system of SVPWM drive can be obtained as shown in figure (15).

4.3 Simulation results:

The no-load test of the SVPWM drive obtained by applied different speed commands to the SVPWM inverter, which is fed a practical induction motor, has the following name plate:

3-phase I.M, 380 volt (line), 550 watt, 4-poles, 50 Hz, 1400 r.p.m, power

factor = 0.78. From these data the following parameters are calculated:

$$T_{rated} = \frac{550 \text{ watt}}{1400 \cdot 2\pi/60} = 3.15 \text{ N.m}$$

$$N_s = 1500 \text{ r.p.m}$$

$$S_{full \text{ load}} = \frac{1500 - 1400}{1500} = 0.067$$

X_s & R_s are measured by using resistance-inductance meter which gives: $X_s = 32 \Omega$, $R_s = 17 \Omega$.

• Calculation of R_r , X_r & X_m : From the equation of motor torque and by using the iteration method, the values of R_r & X_r can be found:

$$T_{rated} = \frac{3 V_p^2 R_r}{5_f \omega_s [(R_s + \frac{R_r}{s})^2 + (X_s + X_r)^2]}$$

The iteration method gives: $R_r = 10 \Omega$, $X_r = 38 \Omega$ (referred to stator).

From the equation of the power factor we can calculate the value of X_m :

Power factor angle

$$\varphi = \pi - \tan^{-1} \frac{R_s + R_r/s}{X_s + X_r} - \tan^{-1} \frac{X_m + X_s + X_r}{R_s + R_r/s}$$

From this equation it found that $X_m = 4805$.

By sequence, the output voltage of the SVPWM inverter and the motor stator current (at no-load condition) are analyzed by using Fourier series, this analysis done by using MATLAB program to obtain the harmonics content of the output voltage and the stator current. The performance parameters (HF, THD) are calculated. The harmonics measurements and the performance parameters of different steps are shown in table (3). And the results steps can be shown in figures (16),(17),(18).

5. System design and implementation:

The standard design of SVPWM driver is a fully digital system based

on microprocessor DSP technology, which used TMS320C24X microcontroller. Because of the difficulty of using TMS 320C24X microcontroller in this design, the operation of this processor can be imitated by some way else. The operation concept of the processor is to calculate (T_o, T_a, T_b) by using software program at real time, therefore instead of that all (T_o, T_a, T_b) periods can be calculated in off-time by using equations (6), (7), (8) over one periodic time for six sectors and its sub-sectors. The calculation data can be stored in any memory device like EPROM. In sequence, these stored data can be read and fed it to the power bridge devices using hardware circuit. This way will be the main strategy of this design, therefore, at first the time periods (T_o, T_a, T_b) of each sector using sub-sector steps equal to (10°) start from (5°) (i.e. $\theta = 5^\circ, 15^\circ, 25^\circ, \dots, 355^\circ$) are calculated. Because of time periods (T_o, T_a, T_b) are identical among the six sectors, the data of one sector can be used to store in the memory and then use it for six sectors. For example the time periods of sector-1 at 90% of rated voltage are shown in table (4). The sampling time (T_s) calculated as following:

$$T_{\text{period}} = \frac{T_{\text{rated period}}}{m} = \frac{1/50\text{Hz}}{0.9}$$

$$= \frac{0.02}{0.9} = 0.0222 \text{ sec.}$$

$$T_{\text{sector}} = \frac{T_{\text{period}}}{6} = \frac{0.0222}{6} = 0.0037 \text{ sec}$$

$$T_s = \frac{T_{\text{sector}}}{6} = \frac{0.0037}{6} = 0.000617 \text{ sec.}$$

5.1 Dead time inclusion:

The MOSFETs devices, which are used as a power bridge, have turn-off delay time called “fall time t_f ” approximately equal to $(3\mu\text{sec})$, but in

other side it have fast turn-on time delay called “rise time t_r ” approximately equal to “ $1\mu\text{sec}$ ”, that may causes serious danger of short-circuit between two complementary devices of one bridge arm during switching mode. Thus, to avoid short-circuit; the incoming turn-on device should be delayed by a certain time delay called “dead-time” typically equal to a few micro seconds [1]. It’s important to mention here that dead-time causes distortion in the output voltage and reduces its magnitude, but it essential for safe operation.

5.2 Memory mapping:

To store all data in a suitable memory device, the data must be arranged in uniform manner. In this design, six different voltage steps (100%, 90%, 80%, 70%, 60%, and 50% of rated voltage) are chosen. Therefore, we have six information groups, by choosing (256 byte) from the memory size for each group, $(6 \times 256 = 1536 \text{ bytes})$ of memory size have to be used. The practical memory device (NEC 2716 EPROM), which has 2Kbyte memory size (2048 byte), is suitable to be used in this design. A (1.5 Kbyte) of the memory size is used to insert the data information by using EPROM programmer kit.

5.3 Clock generation and variation:

Firstly, a controllable clock generator is used to control the speed of memory data reading. For this purpose choose (CD 4046) integrated circuit “I.C.” which is a phase locked loop operation has internal voltage control oscillator “VCO”, this I.C. responses to variable input D.C level in range $0 \rightarrow 5$ volt and outputting variable clock frequency depends on

the time constant of (RC) circuit connected to the I.C. as shown in figure (19). In this design a variable output frequency in range of 50% to 140% rated frequency are assumed. Then the desired clock range is calculated as following:

For 50% rated:

$$T_{\text{period}} = \frac{1}{25\text{Hz}} = 0.04 \text{ sec}$$

- $T_{\text{sector}} = \frac{0.04}{6} = 0.00667 \text{ sec}$

$$T_{\text{clock}} = \frac{0.00667}{256\text{byte}} = 2.6 \times 10^{-5}$$

$$\Rightarrow f_{\text{clock}} = \frac{1}{2.6 \times 10^{-5}} = 38.4 \text{ KHz}$$

For 140% rated:

$$T_{\text{period}} = \frac{1}{70\text{Hz}} = 0.0143 \text{ sec}$$

- $T_{\text{sector}} = \frac{0.0143}{6} = 0.00238 \text{ sec}$

$$T_{\text{clock}} = \frac{0.00238}{256\text{byte}} = 9.3 \times 10^{-6}$$

$$\Rightarrow f_{\text{clock}} = \frac{1}{9.3 \times 10^{-6}} = 107.5 \text{ KHz}$$

Therefore, the clock range is 38.4 kHz → 107.5 kHz, which can be achieved by using (R = 33 kΩ), (C = 10 nf) and variable input D.C level 2.5 → 5 volt. By sequence, the clock frequency fed to a binary counter used as memory address generator, for this purpose a (CD 4040) integrated circuit was used, which have (12 bit) binary counter, (8 bit) of them were used to cover (256 byte) of memory size, as shown in figure (19).

5.4 Output voltage variation:

The method which used to storage different voltage information blocks in the memory, by using different quarters of kilobyte (256 byte) for each, simplified our goal of output voltage variation. This can be achieved by jumping through these memory quarters by selection the desired quarter number. Simply, it can be implemented by using level

encoder circuit as (A/D) converter as shown in figure (19), to convert the command D.C level to the corresponding binary value, which represents the memory quarter number.

- It's important to mention, separate commands of voltage & speed can be used to obtain separate variation of voltage & frequency.

5.5 Data distribution over sectors:

Since, the information data of one sector is stored, thus the data over six sectors must be repeated. For this purpose a (CD 4017) integrated circuit is sufficient to activate sectors one by one, and by using supporter logic circuit consist of "12 AND-gates" & "6 OR-gates", which enable the specific sector and transfer data to the next sector at the end time of previous sector, by sequence, the space vectors will be generated each for its own period time. The circuit diagram of data distribution can be shown in figure (19).

5.6 Gating signals generation:

After generation of space vectors, these signals can be now transferred to the desired power MOSFETs corresponding to each space vector, which can be done by using "6-OR gates have 4-inputs" as shown in figure (19).

5.7 Isolation of gates signal:

To turn-on the power MOSFETs, a gate voltage signal must be applied between the gate and source terminals to push the MOSFET into saturation region. The logical signal generated by the electronic circuit has peak value of (5 volt) with respect to its own ground, therefore, to use this signal the gate signal must be connected to the

MOSFET gate terminal and the ground of the logic circuit to the MOSFET source terminal, this connection leads to short circuit between the source terminals of the six power MOSFETs.

Therefore, the MOSFET gating circuit must be isolated from logic circuit and from other MOSFETs gating circuits. The main types of isolating gating circuits are:

- Pulse transformer isolation, or
- Optocouplers isolation.

In this design the optocouplers isolation circuits are used, which consist of an infrared transmitter diode and silicon photo transistor receiver. The gating signal transfers from the logic circuit to the power circuit by means of infrared light provide an electrical isolation gap.

The gating signal which received from the optocoupler is not enough to turn-on the power devices, therefore, it must amplified before be applied to the power device. A simple electronic circuit is used to amplify gating signal for each power MOSFET. Figure (20) shows two gating circuits of two complementary power MOSFETs.

5.8 (dv/dt) and (di/dt) limitation:

During switching the power devices which connected to an inductive load, the drain current “I_D” raises rapidly in turn-on mode by ratio called (di/dt), and the drain to source voltage “V_{DS}” raises in turn-off mode by ratio called (dv/dt). The safety operation required to keep the operating (di/dt) and (dv/dt) within allowable limits of the power MOSFETs. For this reason a snubber circuit was used to limit the amount

of (dv/dt) and (di/dt). Snubber circuit consist of (RC) circuit called parallel snubber connect in parallel with the MOSFETs, and a series inductance (L_s) called series snubber. The value of these components can be calculated by the following equations [2]:

$$L_s = \frac{V_d * t_r}{I_L} = \frac{300 * 1\mu}{1} = 0.3 \text{ mH}$$

$$C = \frac{I_L * t_f}{V_d} = \frac{1 * 3\mu}{300} = 10 \text{ nf}$$

$$R = 2 \sqrt{\frac{L}{C}} = 2 \sqrt{\frac{0.3mH}{10nf}} = 346.5$$

Where; “V_d” is the power D.C supply, “t_r” is the raising time of the MOSFET (1μsec), “t_f” is the fall time of the MOSFET (3μsec). A three-phase power diode bridge rectifier with (LC) filter used as power D.C source, which supply the power MOSFETs bridge, the power circuit can be shown in figure (21).

5.9 Experimental testing and results:

By applying single phase A.C voltage to the input power bridge of the designed SVPWM drive, a D.C voltage source equals to (300 volt) is gotten, and by using the same practical induction motor, which was used in the simulation tests, then repeating the no-load test steps of different voltages and speeds, we obtained system performance as shown in table (5) and figures (22),(23),(24).

The results obtained by using “hp-harmonic analyzer” and “hp-oscilloscope”.

- Motor name plate: 3-Phase I.M, 380 volt (star connection), squirrel cage, 50 Hz, 4-Poles, 550 watt, and 1400 r.p.m.

6. Conclusions

According to the requirements of safe and reliable variable-speed induction motor operation, the SVPWM technique gives an excellent performance with low harmonic factors (HF) and low of total harmonic distortion (THD), with respect to other types of A.C drives.

1- SVPWM drive treats the inverter as a single unit with eight possible switching states, each state can be represented by a state vector in the two-axis space, the eight state vectors formed a hexagon shape with six sectors. The modulation procedure is accomplished by switching the state vectors in each sector by appropriate time intervals which are calculated in a certain sampling time (T_s).

2- The linear region in SVPWM is larger than other types of PWM technique, where the modulation index approaches to (90.7%) and the maximum output fundamental is ($0.577V_d$). Whereas, in the SPWM the maximum linear modulation index is (78.54%) and the maximum output fundamental is ($0.5V_d$).

3- The harmonic analysis of different output voltage and current, in both simulation and experimental results, gives excellent harmonic reduction and harmonic parameters with respect to square-wave inverter.

4- The total losses of low order harmonics can be minimized by increasing the switching frequency, but in the other hand it may increase the switching losses, therefore, switching frequency must be selected to get minimum total harmonic and switching losses.

5- The SVPWM is a digital modulating technique. Then from the above conclusion and due to simulation and experimental results,

the SVPWM can be considered as the best and the optimum of all PWM technique.

References

- [1] Bimal K. Bose, "Modern Power Electronic and AC Drives", Prentice Hall, 2002.
- [2] Muhammed H. Rashid, "Power Electronics, Circuits, Derives and applications", Pearson Education Inc. 2004.
- [3] Bimal K. Bose, "Power Electronics and Motor Derives Advances and trends", Elsevier Inc, 2006.
- [4] V. Suresh Kumar and P.S. Kannan, "Harmonic Studies In Space Vector PWM Inverter Drive System", IEEE, Power Con, Vol. 1, Page: 123-127, Nov. 2004.
- [5] Saif Thamer Fadhil, "SVPWM Technique for Speed Control of 3-phase Induction Motor", Ms.c. thesis, University of technology, Iraq, 2006.
- [6] Qusay Lotfi Hamdi, "Design of Indirect Field-Oriented Voltage Controller using SVPWM Inverter for Three-phase Induction Motor Drive", Ph.D. thesis, Al-Rasheed collage of engineering, University of technology, Iraq, 2007.
- [7] Wang Nianchun, Xu Jin, "Study Of DTC Torque Ripple Reduction Based On SVPWM", IEEE, Power Con, Vol. 2, Page: 1816-1821, Nov. 2004.
- [8] F. Profumo, A. Boglietti, G. Griva and M. Pastorelli, "Space Vector And Sinusoidal PWM Techniques Comparison Keeping In Account The Secondary

Effects”, IEEE, 0-7803-0835-2/92, 1992.

- [9] Texas instruments, “SVPWM With TMS 320C24X Using Hardware And Software Determined Switching Patterns”, March 1999.

Table(1) phase voltages of the eight states

Space voltage vector	V_{an}	V_{bn}	V_{cn}
$V_0(000)$	0	0	0
$V_1(100)$	$2V_d/3$	$-V_d/3$	$-V_d/3$
$V_2(110)$	$V_d/3$	$V_d/3$	$-2V_d/3$
$V_3(010)$	$-V_d/3$	$2V_d/3$	$-V_d/3$
$V_4(011)$	$-2V_d/3$	$V_d/3$	$V_d/3$
$V_5(001)$	$-V_d/3$	$-V_d/3$	$2V_d/3$
$V_6(101)$	$V_d/3$	$-2V_d/3$	$V_d/3$
$V_7(111)$	0	0	0

Table (4)time periods of 90% ratd(v&f)

Table (2) the eight space vectors

Space vector	V_{qd} -phase
$V_0(000)$	0
$V_1(100)$	$\frac{2}{3} V_d e^{j0^\circ}$
$V_2(110)$	$\frac{2}{3} V_d e^{j60^\circ}$
$V_3(010)$	$\frac{2}{3} V_d e^{j120^\circ}$
$V_4(011)$	$\frac{2}{3} V_d e^{j180^\circ}$
$V_5(001)$	$\frac{2}{3} V_d e^{j240^\circ}$
$V_6(101)$	$\frac{2}{3} V_d e^{j300^\circ}$
$V_7(111)$	0

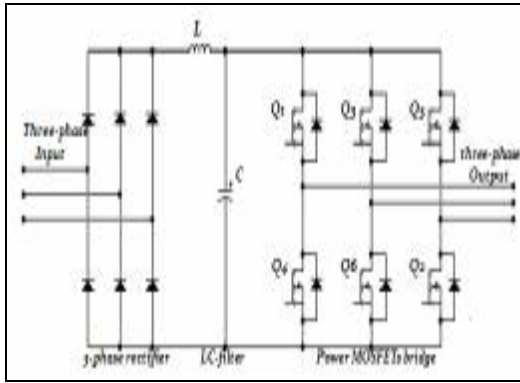
Sub-sectors	90% of rated (V&f)		
	$T_o(\mu\text{sec})$	$T_a(\mu\text{sec})$	$T_b(\mu\text{sec})$
1	63	501	53
2	27	432	158
3	8	351	258
4	8	258	351
5	27	158	432
6	63	53	501

Table (3) phase current harmonics analysis

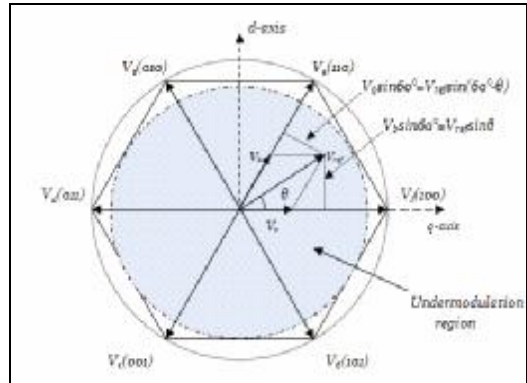
V_{com} %	f_c %	Fundamental Mag. (mA rms)	5 th harmonic		7 th harmonic		THD %
			Mag. mA rms	%HF	Mag. mA rms	%HF	
100	120	500	190	38	65	13	40
100	100	600	200	33.3	60	10	34.8
90	90	590	40	6.8	10	1.7	7
70	70	590	35	5.9	15	2.5	6.5
50	50	560	16	2.9	5	0.9	3

Table (5) phase current harmonics analysis

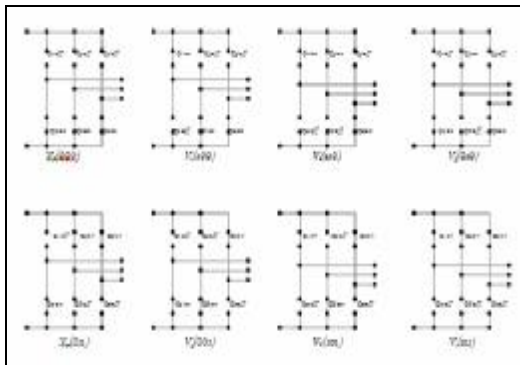
V_{cm} %	f_e %	Fund. Mag. mArms	5 th harmonic		7 th harmonic		THD %
			Mag. mA	%HF	Mag. mA	%HF	
100	120	480	170	35.4	95	20	40.6
100	100	590	200	34	110	18.6	38.7
90	90	587	50	8.5	0	0	8.5
70	70	588	35	6	8	1.4	6.1
50	50	546	16	3	0	0	3



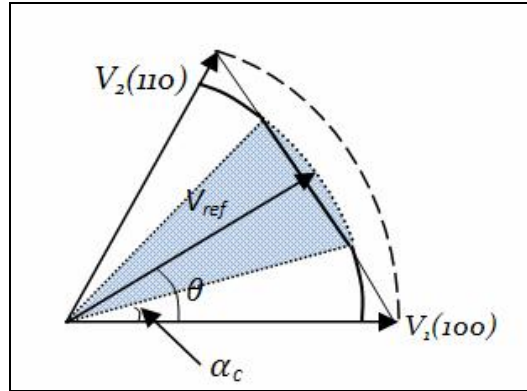
Fig(1) voltage source inverter



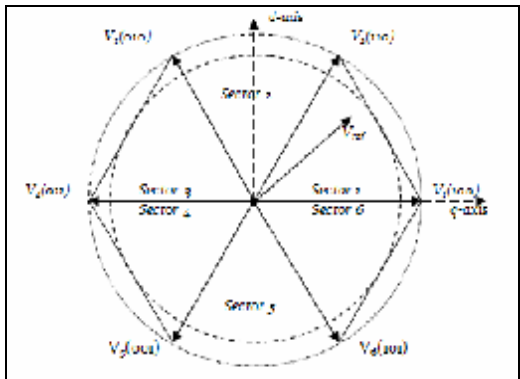
Fig(4) undermodulation region



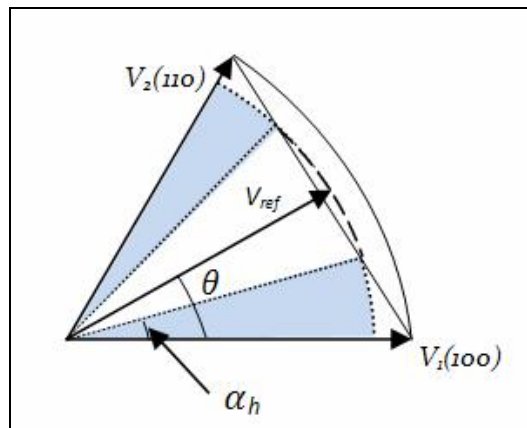
Fig(2) the eight switching states



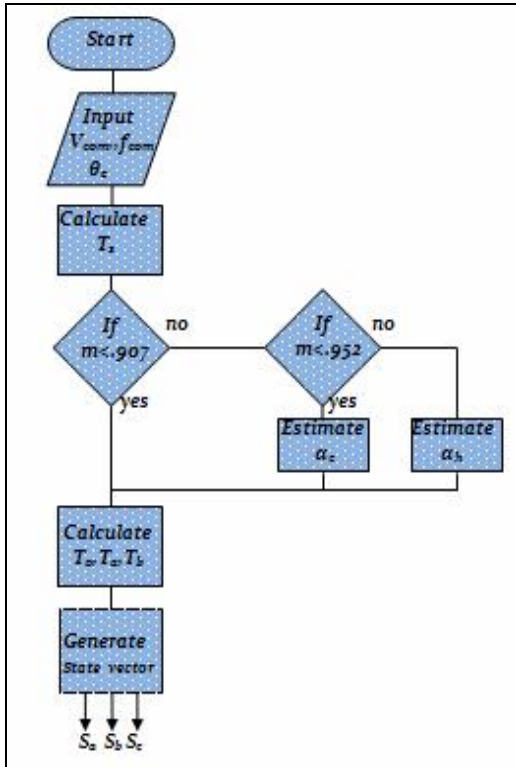
Fig(5) overmodulation region mode-1



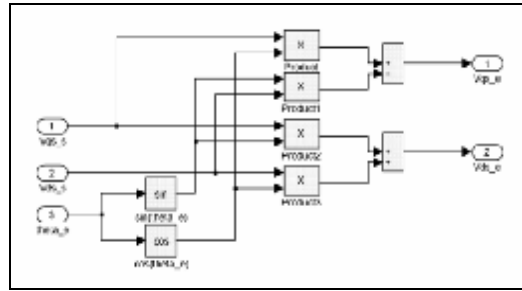
Fig(3) space vectors representation



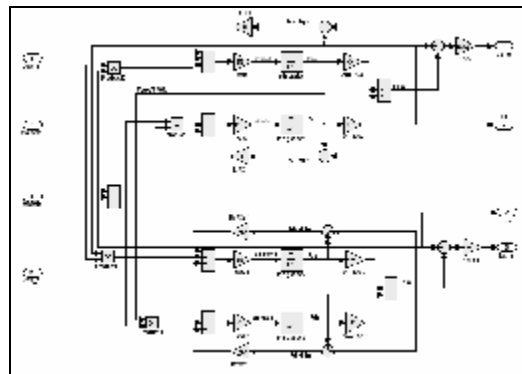
Fig(6) overmodulation region mode-2



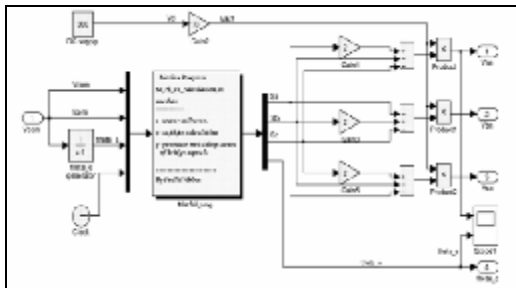
Fig(7) flow chart of SVPWM inverter MATLAB program



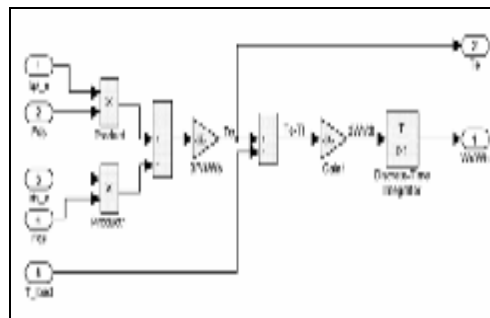
Fig(10) 2-axis stationary to 2-axis rotating



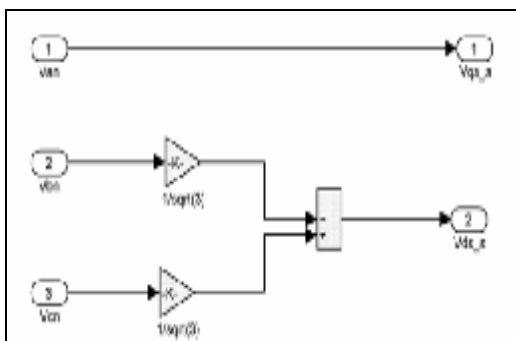
Fig(11) I.M. dynamic model simulation



Fig(8) SVPWM inverter simulation



Fig(12) torque & speed calculation



Fig(9) 3-phase to 2-axis transformation

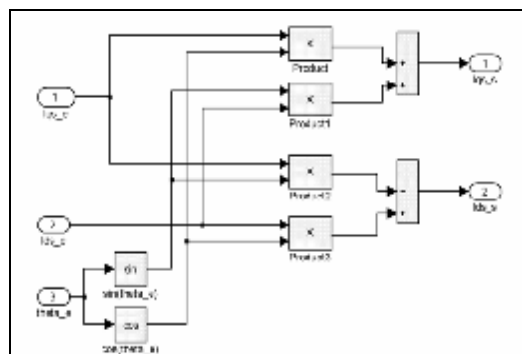


Fig (13) 2-axis rotating to 2-axis stationary

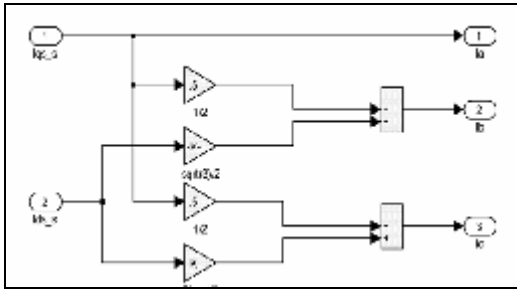


Fig (14) 2-axis stationary to 3-phase

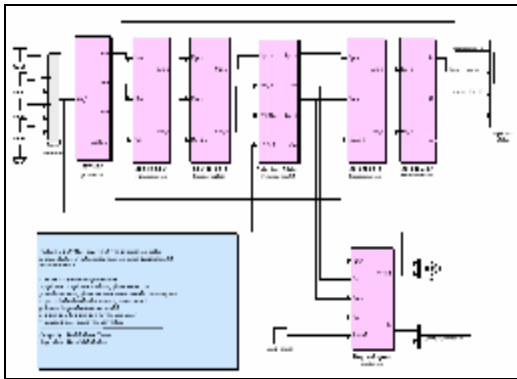


Fig (15) overall system simulation

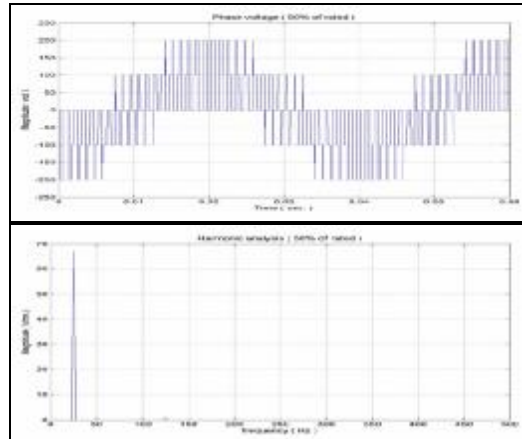


Fig (16-b) phase voltage harmonic analysis of 50% rated (V&f).

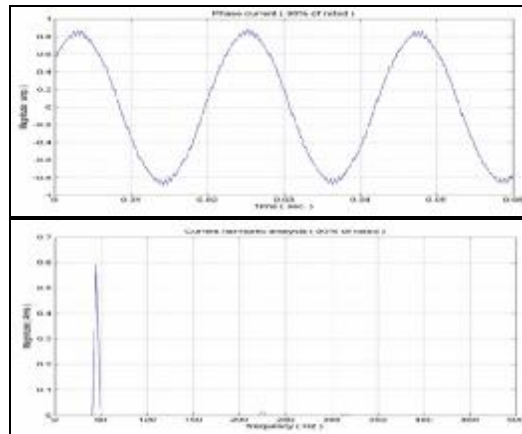


Fig (17-a) phase current harmonic analysis of 90% rated (V&f).

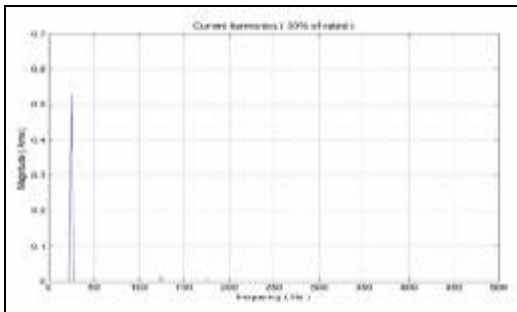


Fig (16-a) phase current harmonic analysis of 50% rated (V&f).

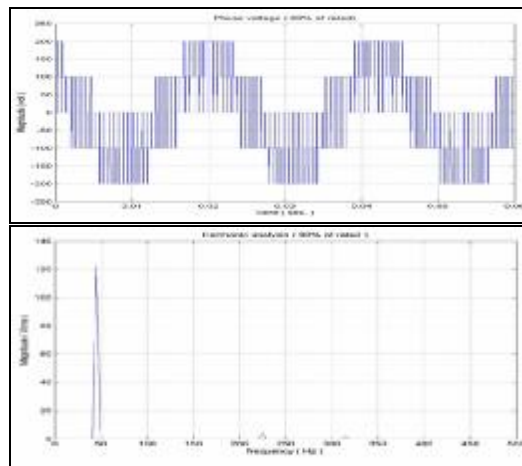


Fig (17-b) phase voltage harmonic analysis of 90% rated (V&f).

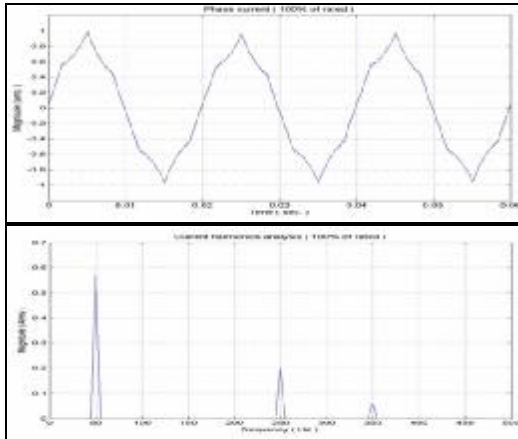


Fig (18-a) phase current harmonic analysis of 100% rated (V&f).

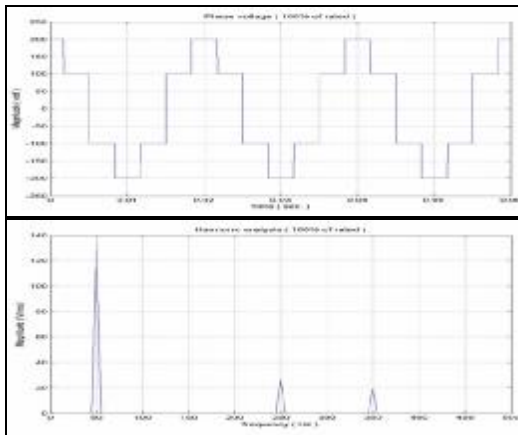


Fig (18-b) phase voltage harmonic analysis of 100% rated (V&f).

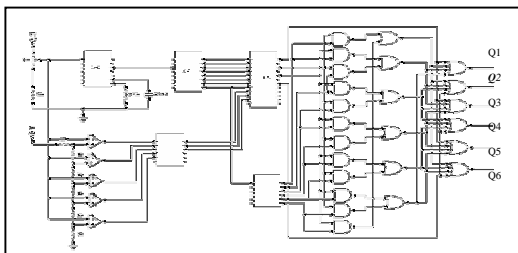


Fig (19) electronic logic circuit

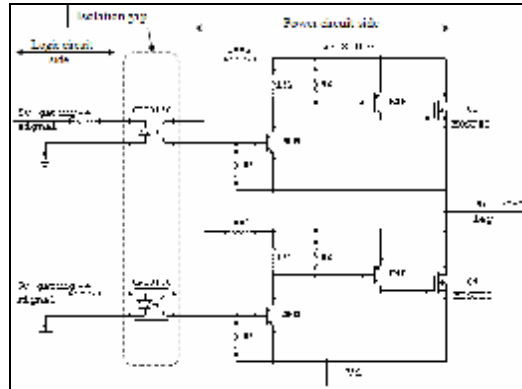


Fig (20) isolation & gating circuit

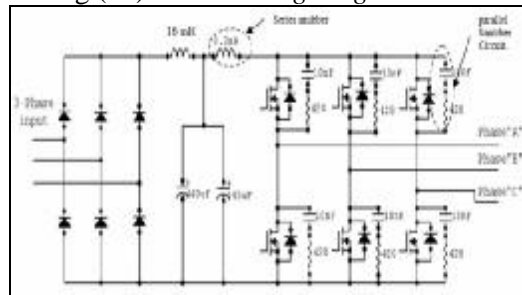


Fig (21) snubber circuit

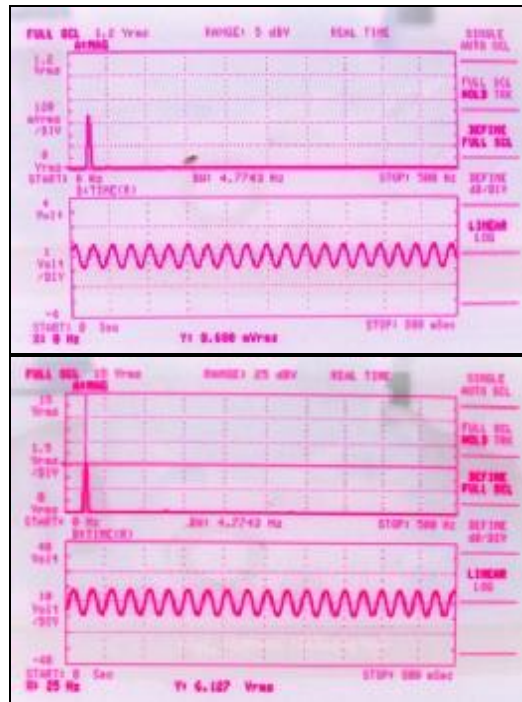


Fig (22) phase current and voltage harmonic analysis of 50% rated (V&f).

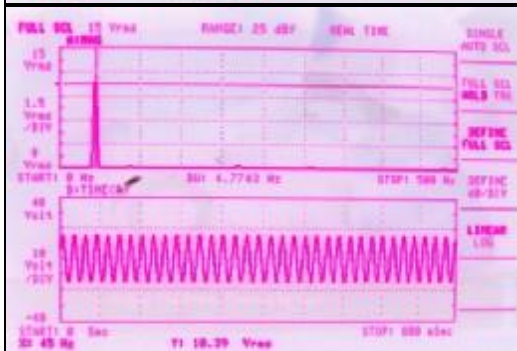
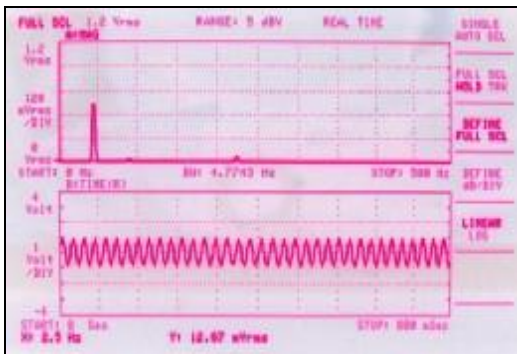


Fig (23) phase current and voltage harmonic analysis of 90% rated (V&f).

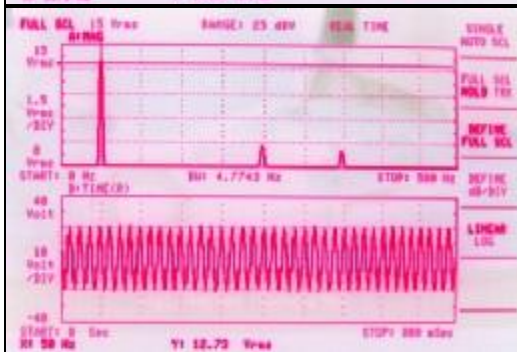
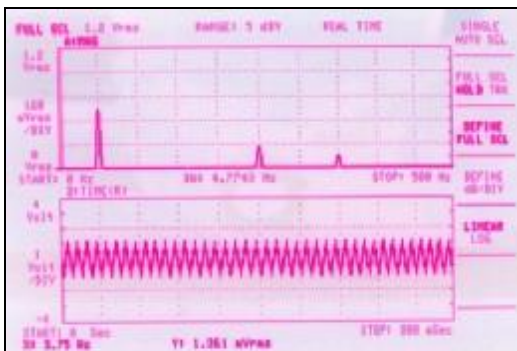


Fig (24) phase current and voltage harmonic analysis of 100% rated (V&f).

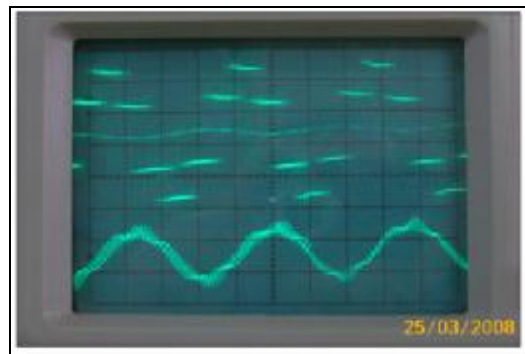


Fig (25) phase current and voltage harmonic analysis of 50% rated (V&f).



Fig (26) phase current and voltage harmonic analysis of 100% rated (V&f).



Picture of SVPWM drive system and work bench